User's Guide
JPL MEaSUREs Gridded Sea Surface Height Anomalies Version 2205

Séverine Fournier, Joshua K. Willis, Emmy Killett, Zheng Qu, and Victor Zlotnicki
Jet Propulsion Laboratory, California Institute of Technology, Pasadena, CA, USA

Abstract

Since 2014, the Jet Propulsion Laboratory has been producing sea surface height grids from nadir satellite radar altimetry (JPL MEaSUREs grids), and in this document we will describe a new version of this gridded data product. These and similar products have found a variety of applications including global mean sea level monitoring, tracking of eddies and Antarctic Circumpolar Current (ACC) fronts, and estimating the transport of the Atlantic Meridional Overturning Circulation, to name just a few.

This document describes the grids that have a latency of a few months (Final product), a few weeks (Interim product), or a few days (Near Real Time product). The latency of the grids is indicated in each file's metadata. **Interim and near real time files will be updated and replaced regularly**. Interim and Near Real Time products have lower accuracy, and **it is the user's responsibility to be aware of the latency in a given file**. Only Final products are recommended for use in climate studies or for purposes that require the highest accuracy.

The technique used to produce these grids has been shown to reproduce wavelengths longer than 350 km near the Equator and 150 km in the ACC region and 250 km in the Gulf Stream region, and provide good agreement with tide gauge data. This version includes improvements such as the use of new versions of input data, an updated corrections applied to the altimeter range including unified choices of sea state bias solutions across satellites, newly computed inter-mission biases, the new DTU21 mean sea surface, a GPS-based Jason-3 orbit, as well as the removal of a strong global mean sea level constraint on the input data. In addition, an error in the calculation of propagation velocities has been corrected, and steps have been taken to reduce discontinuities of the spatial derivatives of sea surface height to provide improved performance in estimates of ocean surface velocity and vorticity.

Credit

Please cite these data as:

Fournier S., Willis J., Killett E., Qu Z. and Zlotnicki V. 2022 JPL MEaSUREs Gridded Sea Surface Height Anomalies Version 2205. PO.DAAC, CA, USA. Dataset accessed [YYYY-MM- DD] at https://doi.org/10.5067/SLREF-CDRV3.

Contents

1. Introduction

Gridded maps of sea surface height (SSH) have found widespread use among the scientific and operational oceanography and climate science community. Willis [2010] demonstrated that SSH maps together with Argo data showed skill in estimating the transport of the upper limb of the Atlantic Meridional Overturning Circulation around 41°N. Sokolov and Rintoul [2007] and Thompson and Sallé [2012] used SSH grids to study fronts of the Antarctic Circumpolar current, and Chelton et al. [2011a] used them to track nonlinear mesoscale eddies based on closed contours of SSH, itself a data product later used in other studies [e.g., Chelton et al., 2011b; Samelson et al., 2014].

Since 2014, the Jet Propulsion Laboratory (JPL) has been producing SSH grids every 5 days from nadir-looking, along-track radar altimeter observations using a technique called ordinary kriging [https://en.wikipedia.org/wiki/Kriging; Cressie and Wikle, 2011, Chapter 4]. The first version of the data (JPL MEaSUREs v1812 grids) were distributed by the Physical Oceanography Distributed Active Archive Center (PO.DAAC), starting in early 2019. In this manual, we describe an updated version of these grids (JPL MEaSUREs v2205). This user guide can be found on the PO.DAAC website (https://podaac-tools.jpl.nasa.gov/drive/files/allData/merged_alt/L4/docs/Documentation_SSH_Measures_V2205_Final.pdf).

Gridded SSH products have a long history in the altimetry community. In a series of papers including LeTraon et al. [1998], Ducet et al. [2000], and LeTraon and Dibarboure [2002], an efficient and accurate method of gridding sea surface heights (SSH) was established using objective mapping techniques [Bretherton et al., 1976]. Numerous studies paid considered removal of long wavelength along track error, and ascertained the accuracy of the technique by sampling numerical model output in the manner a nadir altimeter does, gridding the sampled model, and comparing to the full model grids. The latest version of that series is discussed in Taburet et al. [2018]. Grids produced by various versions of their technique are available from the Copernicus Marine Environment Monitoring Service (CMEMS: https://marine.copernicus.eu) and are sponsored by the Centre National d'Etudes Spatiales of France.

The purpose of the MEaSUREs gridded SSH product is to provide a completely independent set of SSH grids, supported by NASA and using the latest corrections and most up to date altimeter products to produce a self-consistent set of grids with climate-quality accuracy from the mesoscale to the global scale. As observations are ongoing, grids will be updated regularly so that the product maintains relevance and utility.

2. Updates from version 1812

This manual describes the new version (2205) of the MEaSUREs SSH grids produced by JPL. The previous version of the grids was released in 2018 (v1812). In the following, we list the updates and changes made in this version from the previous version and more details on all these changes are provided in the following sections of this document:

- The product made available can have a latency of few months (Final product), few weeks (Interim product), and few days (Near Real Time product). The latency of the product is indicated in each data file's metadata. **The near real time and interim files will be updated regularly** and eventually replaced with Final Products. Final products have the highest accuracy and **it is the users responsibility to ensure they using products with appropriate accuracy and latency**. (See **Section 7**)

- We now use the version 5.1 Goddard Space Flight Center (GSFC) along track data (see **Section 3.1**);
- In the 1812 version of the JPL grids, most of the corrections available in the Radar Altimeter Database System (RADS) were set to default for every satellite. We updated the set of corrections used in this version (see **Section 3.2**);
- We now use data from Sentinel-3B since November 2020 instead of Sentinel-3A;
- Our grids are now referenced to the DTU21 Mean Sea Surface (MSS) instead of the DTU15 MSS (see **Section 4.1**);
- The orbit for the IGDR and OGDR version of the Jason-3 data are switched to the orbit developed by Desai et al. [2020] for better quality data. This imply that three types of output files are generated (final, interim and near real time) instead of two (final and interim) (see **Section 4.2**);
- We are now applying intermission biases between all additional satellites and the GSFC time series (see **Section 4.3**);
- We are no longer adjusting the Global Mean Sea Level (GMSL) of each map to agree with the along-track estimate of GMSL from the reference missions alone (see **Section 5**);
- We are no longer adding explicit orbit-like error to the non-reference satellite missions in the kriging routine (see **Section 5**);
- The number of neighbors was decreased from 6000 to 2000 in the calculation of SSH anomalies at each grid cell. This has shown to decrease the computation time without having significant impact on the quality of the retrieval (see **Section 5**).
- An error in the calculation of feature propagation speeds was corrected (see **Section 5**).
- Parameters used during the kriging process to specify expected variance, length scales and propagation speeds were smoothed to reduce discontinuities in the spatial derivatives of SSH (see **Section 5**).
- Covariance length scales Lx and Ly were chosen to be consistent with the work of Jacobs and Wooten [2013]. On average these scales are slightly larger than those used in previous estimates (see **Section 5**).
- Maps of kriging parameters used to compute SSH grids are now available as ancillary data products (see **Section 5**).

3. Input data

All JPL SSH grids are constructed from along-track data from two simultaneous altimetric satellites. One satellite is TOPEX/Poseidon (T/P), Jason-1, Jason-2, or Jason-3 (reference missions). The other satellite is one of ERS-1, ERS-2, ENVISAT, Cryosat-2, SARAL/AltiKa, Sentinel-3A or Sentinel-3B.

3.1. GSFC data

Most data from the reference missions are obtained from the along track data product generated by the GSFC and distributed by PO.DAAC, entitled "Integrated Multi-Mission Ocean Altimeter Data for Climate Research, version 5.1" (https://podaac.jpl.nasa.gov/dataset/MERGED_TP_J1_OSTM_OST_CYCLES_V51). The satellites used in the GSFC product and the dates over which they are present are listed in **Table 1**. At the time of this manual redaction, GSFC data were available until up to the 22nd of June 2021. The grids will be updated to use the GSFC data as soon as they become available.

Table 1 also shows the corrections applied by GSFC in the production of these data. For more information on these corrections, see the GSFC user manual at https://podaac-tools.jpl.nasa.gov/drive/files/allData/merged_alt/L2/TP_J1_OSTM/docs/v100721.version5.1multialthandbook.pdf.

Changes made in this version 5.1 GSFC along-track dataset compared to the previous version (v4.2) are listed below. More information can be found in the manual (see link above):

- Use of a new orbit (the latest standard std2006 orbit) shows accuracies better than 1 cm for the Jason satellites and 1.5 cm for TOPEX/Poseidon;
- End-of-mission recalibration of the Jason-1 Microwave Radiometer (JMR) included in the GDR-E release enhances the Jason-1 wet troposphere correction;
- Enhancement of the TOPEX Microwave Radiometer (TMR) wet troposphere correction;
- Use of the GOT4.8 (for TOPEX/Poseidon) and GOT4.10 (for the Jason satellites) ocean tide corrections;
- Use of the revised pole tide correction developed by Desai et al. [2015];
- Use of the DTU15 MSS instead of the DTU13 MSS.

Note that T/P data in version 5.1 has the Wallops correction 'un-applied', which partially corrects an error in the early years of the mission [Beckley et al, 2017]. At the time of this writing, T/P retracking and reprocessing is under way and the global mean sea level curve during the TOPEX era is likely to change slightly after reprocessing is complete and the data are assimilated into the grids.

	TOPEX Sides A/B (1992/09/25 - 1999/02/08)/ (1999/02/09 - 2002/05/14)	**Poseidon-1**	**Jason-1** (2002/05/14 – 2008/07/12)	**Jason-2** (2008/07/12 – 2016/03/18)	**Jason-3** (2016/03/18 – 2021/06/22)
Orbit	GSFC std2006 (Altamimi et al., 2016)	GSFC std2006 (Altamimi et al., 2016)	GSFC std2006 (Altamimi et al., 2016)	GSFC std2006 (Altamimi et al., 2016)	GSFC std2006 (Altamimi et al., 2016)
Dry Troposphere	ECMWF Interim Re-analysis	ECMWF Interim Re-analysis	ECMWF operational	ECMWF operational	ECMWF operational
Wet Troposphere	TMR enhanced replacement product (2015)	TMR enhanced replacement product (2015)	GDR_E JMR	GDR_D AMR	GDR_T AMR
Ionosphere	Dual- frequency	Doris/GIM	Dual-frequency	Dual-frequency	Dual-frequency
Inverted Barometer	Dynamic Atmospheric Correction (DAC)	Dynamic Atmospheric Correction (DAC)	ECMWF operational + MOG2D hi- frequency	ECMWF operational + MOG2D hi- frequency	ECMWF operational + MOG2D hi- frequency
Solid Earth Tide	H_Set	H_Set	solid_earth_tide	solid_earth_tide	solid_earth_tide
Pole Tide	Desai et al., (2015)	Desai et al., (2015)	Desai et al., (2015)	Desai et al., (2015)	Desai et al., (2015)
Ocean Tide	GOT4.8	GOT4.8	GOT4.10	GOT4.10	GOT4.10
Load Tide	GOT4.8	GOT4.8	GOT4.10	GOT4.10	GOT4.10
Sea State Bias	Non-parametric (Tran et al., 2010)	Parametric BM4 (Gaspar et al., 1994)	Non-parametric (Tran et al., 2012)	Non-parametric (Tran et al., 2013)	Non-parametric (Tran et al., 2020)
Long-period Tide	Ray & Erofeeva [2014]	Ray & Erofeeva [2014]	Ray & Erofeeva [2014]	Ray & Erofeeva [2014]	Ray & Erofeeva [2014]
Internal Tide	Zaron (2019) V8.1	Zaron (2019) V8.1	Zaron (2019) V8.1	Zaron (2019) V8.1	Zaron (2019) V8.1
Cross-Track gradient	DTU15 MSS	DTU15 MSS	DTU15 MSS	DTU15 MSS	DTU15 MSS
Intermission range bias	23.9 + 0.2 mm (Side B wrt J1/J2) -6.7 mm (Side A wrt adjusted Side B)	26.1 mm wrt J1/J2 (cycles <132) 20.2 mm wrt adjusted TOPEX (cycles >132)	0.2 mm wrt J2	0.0 mm	32.4 mm wrt J2

Table 1: Dates at which the reference missions (TOPEX/Poseidon, Jason-1, 2 and 3) switch in the GSFC dataset and list of corrections used for each satellite (source: https://podaac-tools.jpl.nasa.gov/drive/files/allData/merged_alt/L2/TP_J1_OSTM/docs/v100721.version5.1multialthandbook.pdf).

3.2. RADS data

The data for the second set of satellites is obtained from the RADS database [Scharoo et al., 2013; http://rads.tudelft.nl, https://github.com/remkos/rads/tree/master/doc/manuals]. The exact satellites used depend on the date, as described in **Table 2**.

The specific range of corrections is summarized in **Table 3**, for more information on each correction, refer to the RADS manual (https://github.com/remkos/rads/tree/master/doc/manuals). Few changes were made in the choice of corrections compared to the version 1812 of the JPL MEaSUREs grids. In particular, we use the Tran et al. [2012] and Tran et al. [2020] sea state bias (SSB) correction for Sentinel 3A, 3B and Jason-3 respectively instead of using the CLS non-parametric SSB for Jason-3 and the NOAA hybrid SSB for Sentinel-3A and 3B. We also use now the orbits produced by the Reaper project for ERS-1 and 2 and the GDR orbit for ENVISAT instead of the orbit produced by GFZ in the framework of the ESA Sea Level Climate Change Initiative project.

Data from the reference mission (presently Jason-3, but soon Sentinel-6 Michael Freilich) that has been collected since the most recent datum in the GSFC dataset are obtained from RADS. Maps containing this data are marked either “Interim” or “Near Real Time”, depending on whether the GDR is available (Interim) or only the IGDR or OGDR is available (Near Real Time). For the Near Real Time products, the IGDR/OGDR orbits are replaced with those from Desai et al. [2020] as described in **Section 4.2**. As Sentinel-6 Michael Freilich data is incorporated, NTC products will be treated as GDR, STC products as IGDR and NRT products as OGDR.

JPL grid version	Reference Mission	Additional Satellite (from RADS)	Dates
Final	GSFC	ERS-1	1992/09/25 - 1995/05/14
	GSFC	ERS-2	1995/05/15 - 2002/06/10
	GSFC	ENVISAT	2002/06/11 - 2011/12/31
	GSFC	Cryosat-2	2012/01/01 - 2013/03/14
	GSFC	SARAL/AltiKa	2013/03/15 - 2016/07/03
	GSFC	Sentinel-3A	2016/07/04 - 2018/07/11
	GSFC	Sentinel-3B	*2018/07/12 - 2021/06/22
Interim	GDR Jason-3 (RADS)	Sentinel-3B	*2021/06/23 - 2021/12/07
Near Real Time	IGDR/OGDR Jason-3 (RADS with Desai et al. [2020]'s orbit)	Sentinel-3B	*2021/12/08 - 2022/04/07

*Table 2: Summary of the different data used to compute the final, interim and near real time JPL MEaSUREs grids, at the time of the manual redaction. *Times for Interim and Near Real Time maps are based on the time of initial release of this product. However, as new observations become available, new final, Interim and Near Real Time maps will be added.*

	ERS-1	ERS-2	ENVISAT	Cryosat-2	SARAL/AltiKa	Jason-3	Sentinel-3A	Sentinel-3B
Orbit	Reaper	Reaper or GFZ	GDR-D	GDR-E	GDR-F or GDR-E	GDR-F or GDR-E	GDR-F or GDR-E	GDR-F
Dry Troposphere	ECMWF	ECMWF	ECMWF	ECMWF	ECMWF	ECMWF	ECMWF	ECMWF
Wet Troposphere	Radiometer	Radiometer	Radiometer	ECMWF	Radiometer	Radiometer	Radiometer	Radiometer
Ionosphere	NIC09	JPL GIM or NIC09	Smoothed dual-frequency or JPL GIM or NIC09	JPL GIM	JPL GIM	Smoothed dual-frequency	Smoothed dual-frequency	Smoothed dual-frequency
Inverted Barometer	MOG2d ERA-Int	MOG2d ERA-Int	MOG2d ERA-Int	MOG2d ERA-Int	MOG2d ERA-Int	MOG2d ERA-Int	MOG2d ERA-Int	MOG2d ERA-Int
Solid Earth Tide	Cartwright-Taylor-Edden	Cartwright-Taylor-Edden	Cartwright-Taylor-Edden	Cartwright-Taylor-Edden	Cartwright-Taylor-Edden	Cartwright-Taylor-Edden	Cartwright-Taylor-Edden	Cartwright-Taylor-Edden
Pole Tide	Desai et al. [2015]	Desai et al. [2015]	Desai et al. [2015]	Desai et al. [2015]	Desai et al. [2015]	Desai et al. [2015]	Desai et al. [2015]	Desai et al. [2015]
Ocean Tide	FES2014	FES2014	FES2014	FES2014	FES2014	FES2014	FES2014	FES2014
Load Tide	FES2014	FES2014	FES2014	FES2014	FES2014	FES2014	FES2014	FES2014
Sea State Bias	Parametric BM3	Parametric BM3	CLS non-parametric	CLS non-parametric	Tran et al. [2019]	Tran et al. [2020] non-parametric	Tran et al. [2012] non-parametric	Tran et al. [2012] non-parametric

Table 3: Summary of the corrections selected in the RADS database for the along track data used as inputs for the JPL MEaSUREs grids. Alternative corrections are indicated in case the first choice is not available.

4. Unification of input data

Before gridding the along track data, several changes are made to the input along track data in order to ensure consistency across different missions:

4.1. Mean Sea Surface

First, the mean sea surface (MSS) above which the SSH anomalies (SSHA) are referenced is updated. While all the along-track data used to derive the previous version of the JPL MEaSUREs grids are SSHA computed relative to the DTU15 MSS (ftp://ftp.space.dtu.dk/pub/DTU15/1_MIN/), a more recent mean sea surface is now available (DTU21; ftp://ftp.space.dtu.dk/pub/DTU21/1_MIN). To make use of the newer MSS, we compute the difference between the DTU21 and DTU15 products. This difference is then spatially interpolated onto all along-track data (GSFC and RADS data for each satellite) and then subtracted. This means that the along-track SSH anomalies as well as all the SSH grids (whatever their latency) represent sea surface height above the DTU21 MSS.

4.2. Jason-3 orbit

Depending on the latency of the Jason-3 data retrieved from RADS, the Jason-3 data are either GDR data (~2-month latency), IGDR data (few-day latency) or OGDR data (few-hour latency). In order to improve the precision of the IGDR and OGDR Jason-3 SSH data available in the RADS database, we replace the orbit by the one developed by Desai et al. [2020], an orbit that is computed every 60 seconds using GPS data. This orbit is not part of the orbits available in RADS; daily orbit files were provided by Shailen Desai at JPL. A new orbital position at the time Jason-3 records its SSH along-track data point is estimated by performing a temporal linear interpolation on the Desai et al. [2020] orbit. Then, we simply subtract the orbit that is retrieved from RADS to the SSH along-track values and add the new GPS orbit temporally interpolated. That step is only done on the IGDR and OGDR Jason-3 RADS data and will be the input data to the near-real-time SSH grids (see **Table 2**). As Sentinel-6 Michael Freilich data is incorporated, NTC products will treated as GDR, STC products as IGDR and NRT products as OGDR.

4.3. Intermission biases

In order to ensure that data from different satellites could be combined, we also applied intermission biases to the along-track data from RADS. This provides a consistent input database for the gridding. These biases (**Table 4**) were computed by first regridding the along-track data from GSFC and RADS at each cycle on a 1x3° (latitude x longitude) grid by simply averaging the along-track data falling into each 1x3° pixel; and then computing the average map of the difference between the GSFC and RADS grids across the time period of each additional satellite (**Figure 1**). Finally, the intermission biases represent the area-weighted mean of each map of the differences (**Table 4**). These biases were computed after switching the MSS from DTU15 to DTU21 and after replacing the RADS IGDR and OGDR Jason-3 orbit.

RADS dataset	Intermission Bias GSFC/RADS (cm)
ERS-1	0.54
ERS-2	0.67
ENVISAT	0.67
Cryosat-2	1.37
SARAL/AltiKa	0.96
Jason-3	0.93
Sentinel-3A	0.83
Sentinel-3B	0.67

Table 4: Intermission biases between the GSFC time series from the reference missions TOPEX, Jason-1, 2 and 3 and RADS dataset from ERS-1, 2, ENVISAT, Cryosat-2, SARAL/AltiKa, Jason-3, Sentinel-3A and 3B respectively.

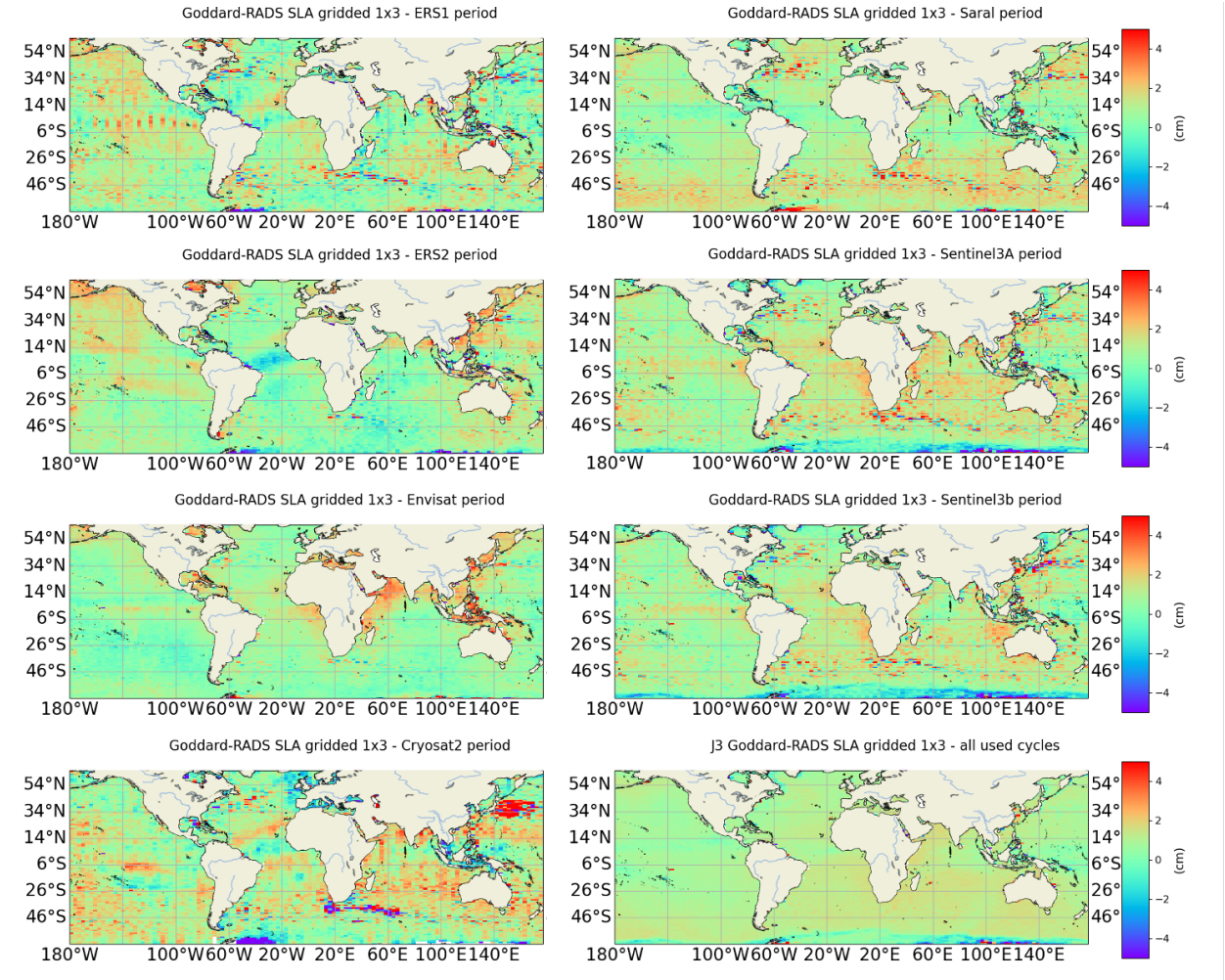

*Figure 1: Average map of the difference between the GSFC and RADS grids across the time period of ERS-1, ERS-2, ENVISAT, Cryosat-2, SARAL/AltiKa, Jason-3, Sentinel-3A and Sentinel-3B. The intermission biases shown in **Table 4** correspond to the spatial mean value of these differences for each satellite.*

4.4. Along-track filtering

After unifying along-track data across satellite missions, the along track data are smoothed with a 19-point filter: the filter is a sinc function multiplied by a Blackman window, with cutoff frequency of 0.11 Hz. The coefficients used are listed below (the filter is symmetric, and values below are for right-side coefficients, starting from the center point coefficient, to the rightmost one):

[0.222115, 0.196706, 0.134041, 0.0646945, 0.0150775, -0.00675300, -0.00907955, -0.00461792, -0.00110582, -2.06117e-05]

Figure 2 shows the filter response against simulated altimeter data (bottom panel). The "RADS smoothed" (second panel from the top) signal is constructed out of a random RADS along track SSH, using a low pass Butterworth filter (see filter response function at top panel) with cutoff around 0.1 HZ (10 points). A random noise with 6 cm standard deviation is added to the "RADS smoothed" to create simulated altimeter data to test the filter response (third panel from the top).

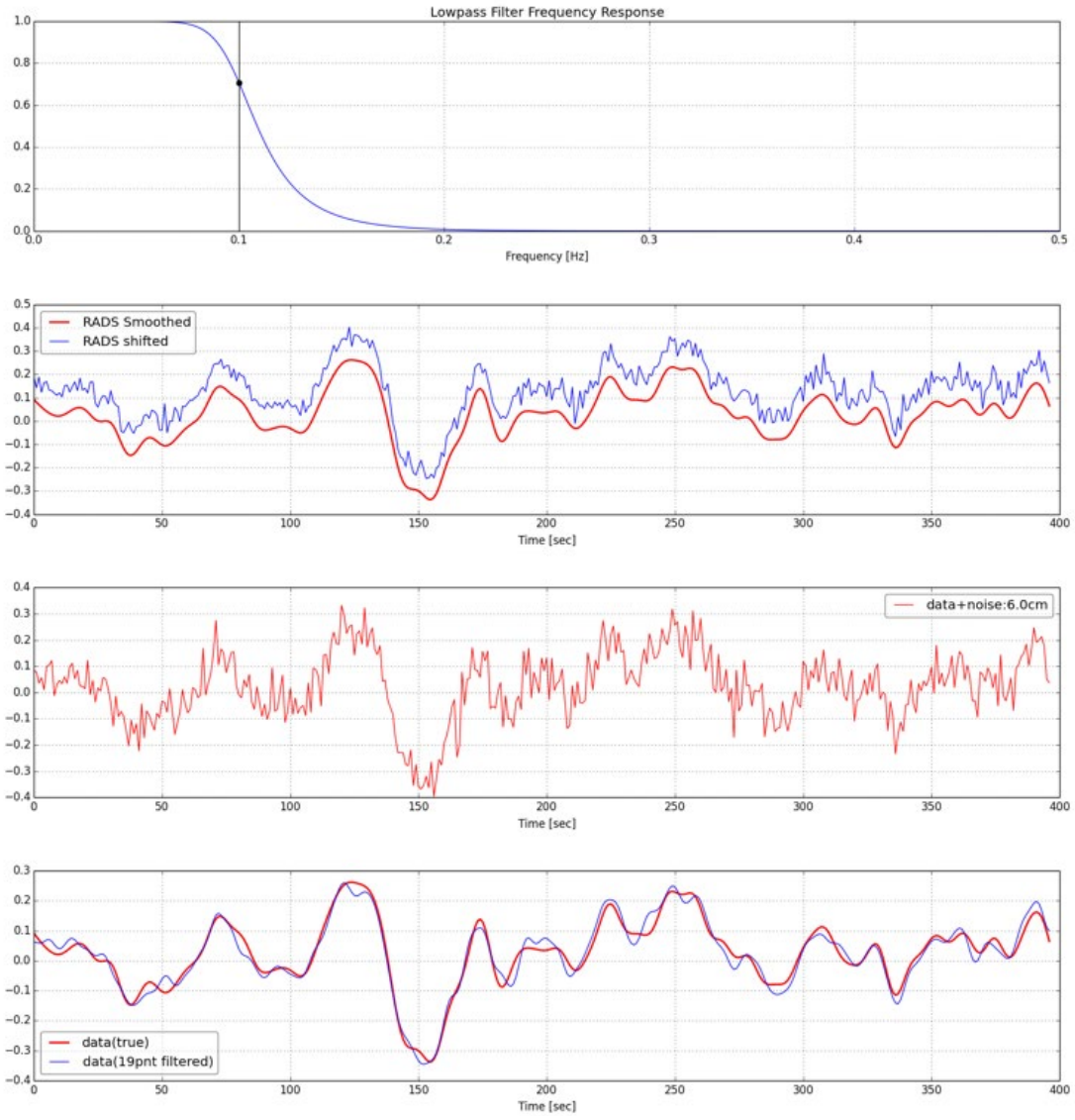

Figure 2: (top panel) Response of a low pass Butterworth filter with cutoff around 0.1 Hz (10 points); (second panel) RADS smoothed data that is constructed out of a random RADS along track data using the low pass Butterworth filter shown above—curves are offset for clarity; (third panel) simulated altimeter data (a random noise with 6 cm standard deviation is added to the RADS smoothed data); (bottom panel) 19-point filter (sinc function multiplied by a Blackman window) response against simulated altimeter data.

4.5 Removal of Spurious Tracks

On visual inspection of the along-track data, a small number of tracks were identified that still had large errors remaining. To avoid introducing these into the grids, the daily along-track files containing these tracks were removed. **Table 5** below lists the satellites and dates of the daily files with questionable data that have been removed.

Satellite/Source	Dates with Erroneous Data
ERS-1	1995/03/19-1995/03/21 1995/11/14
ERS-2	1996/01/15 1996/08/21 1996/12/03 1992/02/10 1997/02/14-1997/02/18 1997/09/16 2000/05/30 2000/07/15-2000/07/16 2000/12/05-2000/12/06 2001/03/31 2001/10/21-2001/10/22 2001/11/06-2001/11/07 2001/11/24 2002/03/24
ENVISAT	2002/09/25-2002/09/27 2002/10/02 2002/10/10 2003/10/29-2003/10/31 2007/06/30-2007/07/01
Sentinel-3A	2017/09/06
GSFC (TOPEX)	1997/06/07 2000/01/12
GSFC (Jason-1)	2003/04/16 2005/09/18

Table 5: List of the dates of daily files with questionable data that were discarded.

4.6. Summary

After these four modifications (MSS swap on all data, orbit swap on the RADS IGDR and OGDR Jason-3 data, intermission biases application and along-track filtering), the then homogenized along-track data are stored as daily files for each satellite. These daily along-track data will soon be released as an independent dataset and will be distributed by PO.DAAC.

5. Gridding method

Once along-track data is homogenized, a technique called ordinary kriging [https://en.wikipedia.org/wiki/Kriging; Cressie and Wikle, 2011, Chapter 4] is used to produce gridded SSH maps on a 1/6th degree grid. Although the output grid has a 1/6th degree resolution, the kriging itself is computed on a set of "grid cells" with 1-degree spacing, globally. Kriging relies on the specification of a covariance function for each location. The MEaSUREs grids use a covariance function with the following form:

$$Cov_{ij} = \langle \mathrm{h}(x_i, y_i, t_i)\, \mathrm{h}((x_j, y_j, t_j)) \rangle \quad (2)$$

where h(x,y,t) is SSH at horizontal position x, y, and time t, and the angle brackets < > denote the expected value operator, implemented here as average over pairs of SSH observations separated by in space by dx and dy, and separated in time by dt. Given this generalization, estimates of the covariance function can be calculated from SSH observations and modeled. Here we follow the functional form of the covariance function suggested by Le Traon et al. [1998]:

$$Cov = \mathrm{var} \times \mathrm{b} \times \mathrm{e}^{-r_{ij} - (\frac{dt_{ij}}{Lt})^2} \quad (3).$$

While functional form remains the same for all gridding locations, several of the key parameters in equation (3) are allowed to vary slowly over space and time. In equation (3), the

- var = local variance. This changes regionally and is estimated from 29 years estimate of gridded SSH maps, made without propagation velocities, as discussed below. An *a priori* estimate of var was made using along-track data, but the variance across gridded maps provides a more realistic estimate of local variance explained by the kriging and is therefore used in the final kriged product. Before kriging, the map is smoothed spatially to reduce discontinuities in the final SSH grids (See **Figure 3**). A map of this value is available as an ancillary product;

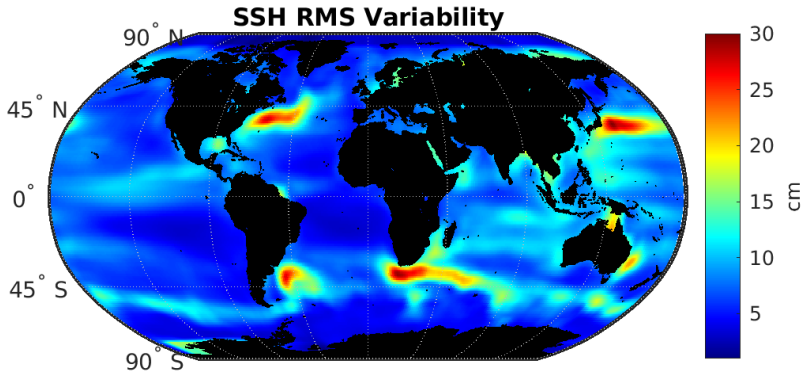

Figure 3. RMS Variability of SSH computed from Grids made without propagation and smoothed.

- $b = 1 + r + \frac{r^2}{6} - \frac{r^3}{6}$;
- $r = a\sqrt{(\frac{dx - Cx\, dt}{Lx})^2 + (\frac{dy - Cy\, dt}{Ly})^2}$ with dx = x_i-x_j, likewise for dy and dt;

- a = 3.3369;
- Lt = 15 days;
- Lx and Ly are length scales in the zonal and meridional directions determined by fitting the above function to along-track covariance functions determined from historical along track repeat altimetry data in Jacobs [2013] (**Figure 4**). These maps are smoothed slightly to avoid discontinuities between adjacent grid cells in the SSH grids. Maps of Lx and Ly are available as ancillary products.

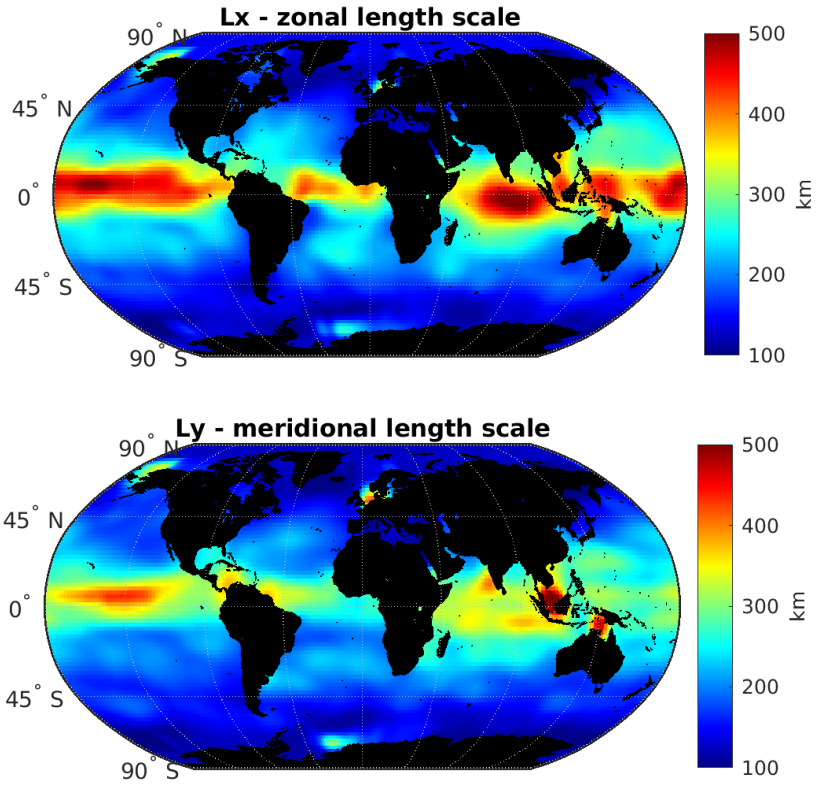

Figure 4: (top) Lx from Jacobs [2013] and (bottom) Ly.

- Cx and Cy are components of velocity for features that propagate through in the ocean. The propagation velocities are determined as follows: in a first step, Cx, Cy are set to zero and the complete dataset is used to generate grids sampled every 1/6th of a degree and 5 days. In a second step, Cx and Cy are determined from successive grids by decomposing into circles, whose radius is the square root of Lx*Ly. The two circles of gridded values are shifted by up to 1 degree of offset in all directions. The correlation coefficient between the shifted circles is computed and Cx and Cy are determined by the relative position with maximum cross correlation. The Cx and Cy fields are smoothed spatially, and averaged across 25 days to ensure smoothly changing propagation speeds and to avoid discontinuities between grid cells in the SSH grids. The final step reruns the whole gridding computation using the Cx and Cy maps thus determined (**Figure 5**). Maps of Cx and Cy are available as an ancillary data product.

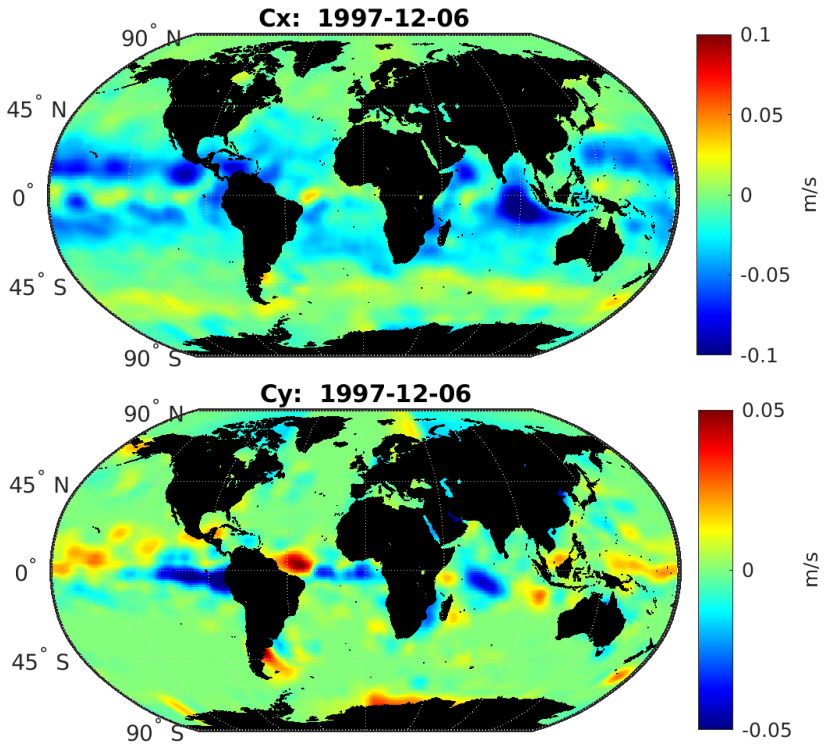

Figure 5: Propagation velocity components Cx and Cy for 06 Dec 1997 (a new set of Cx, Cy is computed for each 5-day map).

Given the covariance function in equation (3), the estimation of SSH(x, y, t), is the linear combination given by the sum of SSH(x_i, y_i, t_i) * w_i(x_i, y_i, t_i) where the vector w of weights w_i is estimated by least squares as:

$$\begin{pmatrix} w \\ \mu \end{pmatrix} = \begin{pmatrix} D + E_{ij} & N \\ N^T & 0 \end{pmatrix}^{-1} \begin{pmatrix} G \\ 1 \end{pmatrix} \quad (4)$$

Where:

- D is a matrix containing the covariance function defined in equation (3) and evaluated between the positions of each data point used in the kriging at (x_i, y_i, t_i) with every other data point (x_j, y_j, t_j);
- E_{ik} is diagonal, and assumed to be 16 cm^2 for the TOPEX, Jason-1, 2, 3 satellites, and 36 cm^2 for the ERS-1, 2, ENVISAT, SARAL/AltiKa, Cryosat 2, Sentinel 3A and 3B satellites.
- G is a column vector containing the covariance function evaluated at the location of interpolation (the grid node, or the center of each grid cell) and each of the surrounding data points;
- N is a column vector of appropriate length, containing values of "1" for each element;

Mapping uncertainties, σ (labeled "SLA_ERR" in the data product) are estimated using the kriging standard error as:

$$\sigma = \sqrt{var - (G^T\ 1) \begin{pmatrix} D + E_{ij} & N \\ N^T & 0 \end{pmatrix}^{-1} \begin{pmatrix} G \\ 1 \end{pmatrix}}. \quad (5)$$

Using equation (4), the product of the inverted matrix and data-grid covariance vector can be simplified as follows:

$$\sigma = \sqrt{var - \ (G^T\ 1)\begin{pmatrix} w \\ \mu \end{pmatrix}}, \quad (6)$$

which is how mapping uncertainty is calculated in practice.

To avoid combining data in different 'correlation zones' (for example, Atlantic and Pacific across Panama), different zones were defined (see **Figure 6**). In solid color zones from **Figure 6**, data cannot be combined with data from another color zone, but can be combined with data from white zones. Data from dotted color zones cannot be combined with data from any other zone (including white zones).

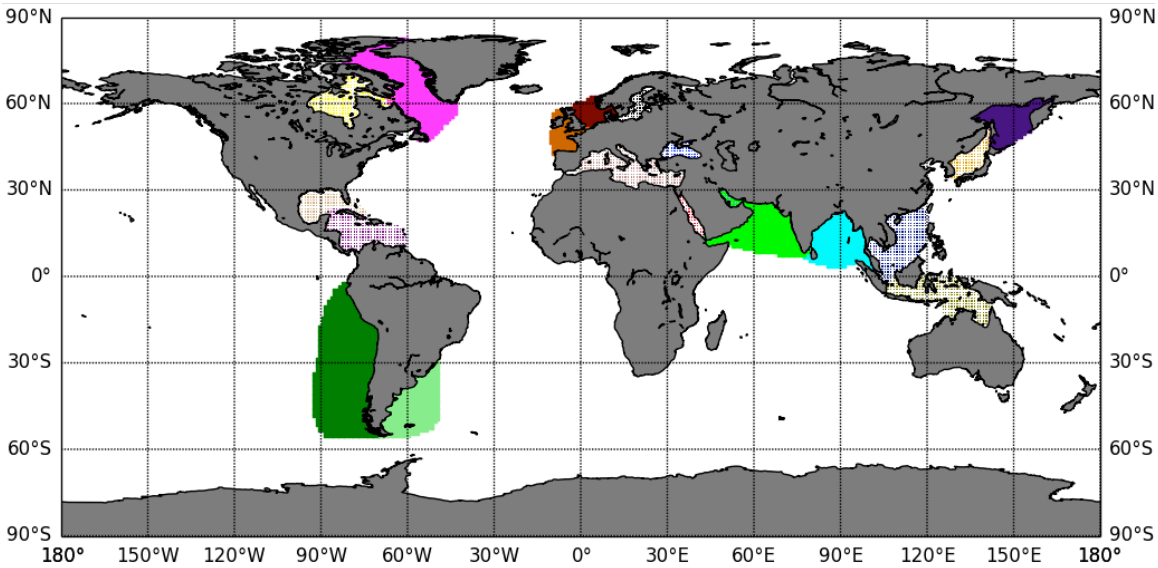

Figure 6: Each color corresponds to a zone that cannot combine data with any other zone.

The matrices do not contain all the global data distribution, but only data in two space windows: the inner window has a 400 km radius, the outer window 1050 km radius, and the time window is 30 days. All data in the inner window are used, 1 data point every 3 in the outer window are used. The matrix is inverted for all points inside a 1° box in both latitude and longitude to compute the weight vector *w*.

In the far northern part of the Hudson Bay, ocean tides aren't accurate enough so we are discarding the data in that region. However, data in the southern part of the Hudson Bay are still used allowing to compute SSHA in grid points in all the Bay. The box where data are excluded is: Longitude: 276° - 288° E, Latitude: 64.5° - 71° N.

6. Coverage and resolution

The grids are given every 5 days on a 1/6th of a degree grid. The actual resolution is as illustrated in the Accuracy Assessment sections of the former user guide available at: https://podaac-tools.jpl.nasa.gov/drive/files/allData/merged_alt/L4/docs/alti-gridding-jpl-PODAAC-UserGuide_20200227.pdf. In the ACC region wavelengths longer than 150 km with 4 cm overall RMS,

in the Gulf Stream region wavelengths longer than 225 km with 9.5 cm RMS, and in the equatorial region wavelengths longer than 350 km with 4.4 cm RMS.

7. Difference between “final”, “interim” and “near real time” grids

The difference between “final” product, “interim” product and “near real time” product (indicated in the “latency” global attribute in the metadata for each file) is the data source for the Jason series of satellites. In the final grids, the Jason series data come from the GSFC processed data mention above, which is usually delayed by ~6 months in order to yield the highest accuracy product. In the “interim” and “near real time” grids, the Jason-3 data are obtained from the RADS system using the set of corrections presented in **Table 2**. While the interim grids use the GDR version of the Jason-3 along track data for the reference mission (with a latency of ~2 months), the near real time grids use the IGDR or OGDR version of the Jason-3 along track data (with a latency of few days to few hours respectively). As explained in **Section 4.2**, the orbits of the IGDR and OGDR Jason-3 along track data were replaced by the ones developed by Desai et al. [2020] that rely on GPS data. The Near Real Time and Interim grids will be updated regularly and eventually replaced with Final grids.

8. Format

The filenames are of the form ssh_grids_v2205_1992100712.nc , where the date of the midpoint of the interpolation is year 1992, month 10, day 07, hour 12 noon. The extension ‘nc’ refers to the netCDF format. The version number (2205) refers to the year and month when the code was frozen (May 2022).

The data files are NetCDF, CF compliant. The attributes can be seen below:

```
File "ssh_grids_v2205_2021060512.nc"; File type: NetCDF-4/CDM:
netcdf ssh_grids_v2205_2021060512 {
dimensions:
        Time = UNLIMITED ; // (1 currently)
        Latitude = 960 ;
        Longitude = 2160 ;
        nv = 2 ;
variables:
        float Lon_bounds(Longitude, nv) ;
                Lon_bounds:units = "degrees_east" ;
                Lon_bounds:comment = "longitude values at the west and east bounds of each pixel." ;
        float Longitude(Longitude) ;
                Longitude:standard_name = "longitude" ;
                Longitude:units = "degrees_east" ;
                Longitude:point_spacing = "even" ;
                Longitude:long_name = "longitude" ;
                Longitude:axis = "X" ;
                Longitude:bounds = "Lon_bounds" ;
        float Lat_bounds(Latitude, nv) ;
                Lat_bounds:units = "degrees_north" ;
                Lat_bounds:comment = "latitude values at the north and south bounds of each pixel." ;
        float Latitude(Latitude) ;
                Latitude:standard_name = "latitude" ;
```

Latitude:units = "degrees_north" ;
Latitude:point_spacing = "even" ;
Latitude:long_name = "latitude" ;
Latitude:axis = "Y" ;
Latitude:bounds = "Lat_bounds" ;
float Time(Time) ;
Time:standard_name = "time" ;
Time:long_name = "Time" ;
Time:units = "Days since 1985-01-01 00:00:00" ;
Time:calendar = "gregorian" ;
Time:bounds = "Time_bounds" ;
Time:axis = "T" ;
float Time_bounds(Time, nv) ;
Time_bounds:units = "Days since 1985-01-01 00:00:00" ;
Time_bounds:comment = "Time bounds for each time value, same value as time variable. The time variable is defined on points instead of on bounding boxes." ;
float SLA(Time, Latitude, Longitude) ;
SLA:units = "m" ;
SLA:_FillValue = 9.96921e+36f ;
SLA:long_name = "Sea Level Anomaly Estimate" ;
SLA:standard_name = "sea_surface_height_above_sea_level" ;
SLA:coordinates = "Time Longitude Latitude" ;
SLA:scale_factor = 1.f ;
SLA:add_offset = 0.f ;
SLA:alias = "sea_surface_height_above_sea_level" ;
float SLA_ERR(Time, Latitude, Longitude) ;
SLA_ERR:units = "m" ;
SLA_ERR:_FillValue = 9.96921e+36f ;
SLA_ERR:long_name = "Sea Level Anomaly Error Estimate" ;
SLA_ERR:coordinates = "Time Latitude Longitude" ;
SLA_ERR:scale_factor = 1.f ;
SLA_ERR:add_offset = 0.f ;

// global attributes:
:Conventions = "CF-1.6" ;
:ncei_template_version = "NCEI_NetCDF_Grid_Template_v2.0" ;
:Institution = "Jet Propulsion Laboratory" ;
:geospatial_lat_min = -79.91666f ;
:geospatial_lat_max = 79.91666f ;
:geospatial_lon_min = 0.08333334f ;
:geospatial_lon_max = 359.9167f ;
:time_coverage_start = "2021-06-05" ;
:time_coverage_end = "2021-06-05" ;
:date_created = "2022-05-18T00:05:09.642709" ;
:title = "Sea Level Anomaly Estimate based on Altimeter Data, final product (replaced interim version)." ;

:short_name = "SEA_SURFACE_HEIGHT_ALT_GRIDS_L4_2SATS_5DAY_6THDEG_V_JPL2205" ;
:long_name = "MEaSUREs Gridded Sea Surface Height Anomalies Version 2205" ;
:summary = "Sea level anomaly grids from altimeter data using Kriging interpolation, which gives best linear prediction based upon prior knowledge of covariance. " ;
:DOI = "10.5067/SLREF-CDRV3" ;
:version_number = "2205" ;
:Data_Pnts_Each_Sat = "{\"16\": 766327, \"1007\": 676887}" ;
:source_version = "commit ad8fdfbffc5581946ae8e9ea13699e2d6dcadba9" ;
:SLA_Global_MEAN = 0.0588358543447781 ;
:SLA_Global_STD = 0.0859100771618066 ;
:latency = "final" ;
}

The interim and near real time grids can be identified by looking into the metadata. Below are examples of the global attributes in the metadata for an interim and a near real time files:

Interim file: netcdf ssh_grids_v2205_2021121212 {
// global attributes:
:Conventions = "CF-1.6" ;
:ncei_template_version = "NCEI_NetCDF_Grid_Template_v2.0" ;
:Institution = "Jet Propulsion Laboratory" ;
:geospatial_lat_min = -79.91666f ;
:geospatial_lat_max = 79.91666f ;
:geospatial_lon_min = 0.08333334f ;
:geospatial_lon_max = 359.9167f ;
:time_coverage_start = "2021-12-12" ;
:time_coverage_end = "2021-12-12" ;
:date_created = "2022-05-18T00:05:10.155377" ;
:title = "Sea Level Anomaly Estimate based on Altimeter Data, interim product (replaced near real time version)." ;
:short_name = "SEA_SURFACE_HEIGHT_ALT_GRIDS_L4_2SATS_5DAY_6THDEG_V_JPL2205" ;
:long_name = "MEaSUREs Gridded Sea Surface Height Anomalies Version 2205" ;
:summary = "Sea level anomaly grids from altimeter data using Kriging interpolation, which gives best linear prediction based upon prior knowledge of covariance. " ;
:DOI = "10.5067/SLREF-CDRV3" ;
:version_number = "2205" ;
:Data_Pnts_Each_Sat = "{\"4\": 764173, \"1007\": 683403}" ;
:source_version = "commit ad8fdfbffc5581946ae8e9ea13699e2d6dcadba9" ;
:SLA_Global_MEAN = 0.0710132083647889 ;
:SLA_Global_STD = 0.0975199312202698 ;
:latency = "interim" ;
}

Near real time file: netcdf ssh_grids_v2205_2022020512 {
// global attributes:
:Conventions = "CF-1.6" ;

:ncei_template_version = "NCEI_NetCDF_Grid_Template_v2.0" ;
:Institution = "Jet Propulsion Laboratory" ;
:geospatial_lat_min = -79.91666f ;
:geospatial_lat_max = 79.91666f ;
:geospatial_lon_min = 0.08333334f ;
:geospatial_lon_max = 359.9167f ;
:time_coverage_start = "2022-02-05" ;
:time_coverage_end = "2022-02-05" ;
:date_created = "2022-05-18T00:05:10.702208" ;
:title = "Sea Level Anomaly Estimate based on Altimeter Data, near real time product." ;
:short_name = "SEA_SURFACE_HEIGHT_ALT_GRIDS_L4_2SATS_5DAY_6THDEG_V_JPL2205" ;
:long_name = "MEaSUREs Gridded Sea Surface Height Anomalies Version 2205" ;
:summary = "Sea level anomaly grids from altimeter data using Kriging interpolation, which gives best linear prediction based upon prior knowledge of covariance. " ;
:DOI = "10.5067/SLREF-CDRV3" ;
:version_number = "2205" ;
:Data_Pnts_Each_Sat = "{\"4\": 515219, \"1007\": 376257}" ;
:source_version = "commit ad8fdfbffc5581946ae8e9ea13699e2d6dcadba9" ;
:SLA_Global_MEAN = 0.068516662069007 ;
:SLA_Global_STD = 0.0915344894049288 ;
:latency = "near real time" ;
}

9. Accuracy assessment

The accuracy for the predecessor of this dataset was assessed in the previous user guide available at: https://podaac-tools.jpl.nasa.gov/drive/files/allData/merged_alt/L4/docs/alti-gridding-jpl-PODAAC-UserGuide_20200227.pdf. Also, the v1812 JPL MEaSUREs grids were used in scientific studies. For example, Hamlington et al. [2019a] used the JPL grids to the modes of variability of sea level at a global scale while Hamlington et al. [2019b] used the grids to study the natural and forced patterns of sea level rise during the altimeter era. Future assessments of this new product will happen later on.

Figure 7 shows the global mean sea level estimated by averaging the grids over the domain between 66° of latitude. This gives comparable results to the along-track based estimate of GMSL computed using the technique of Beckley et al. [2017] and available from PODAAC from https://podaac-tools.jpl.nasa.gov/drive/files/allData/merged_alt/L2/TP_J1_OSTM/global_mean_sea_level/GMSL_TPJAOS_5.1_199209_202202.txt. Note that maps prior to 1 Jan 1993 should not be used for global mean sea level studies, due to uncorrected errors in TOPEX/Poseidon.

Also shown in **Figure 7** is an estimate of the RMS uncertainty computed as the square root of the area-weighted average of the mapping uncertainty. This area average is computed between 66° of latitude to correspond with the reference mission coverage. The value increases at times when one of the two satellites becomes unavailable or its sampling pattern changes significantly. One example of this occurs at the very end of 1993. In late 1993, for about 4 months, ERS-1 was put into a 3-day repeat orbit ("the ice phase": http://www.deos.tudelft.nl/ers/phases/). This means that the spacing between ground tracks at the equator was around 800-900 km causing an increase error at short wavelengths compared with the rest of the time series.

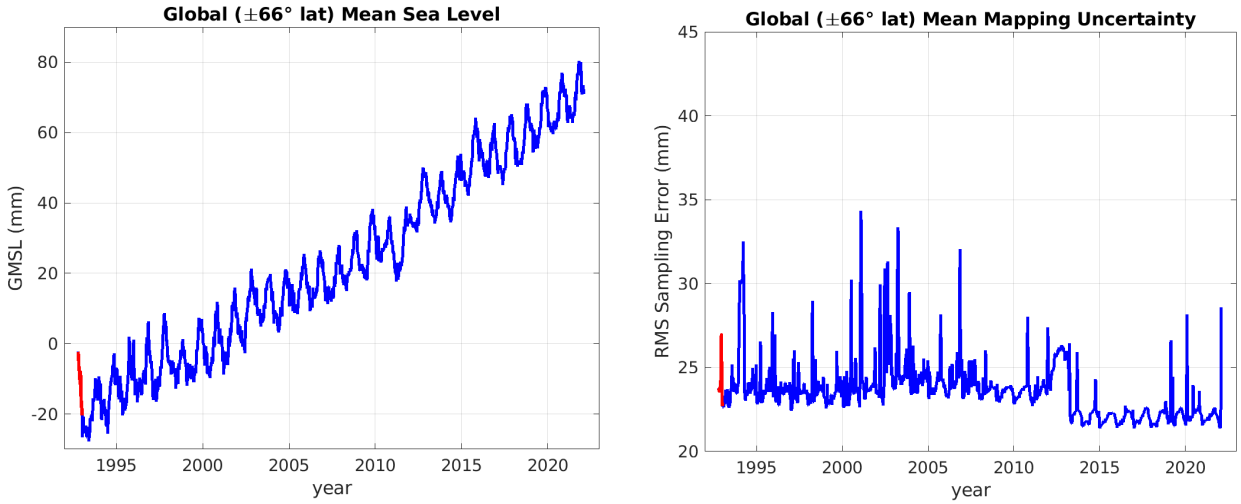

Figure 7: (left) Global mean sea level computed from the grids. (right) Globally-averaged mapping uncertainty from the grids. Red colors show times before 1993, a period where the grids should not be used for GMSL studies due to uncorrected instrument errors during this period.

10. Acknowledgements

The research was carried out in part at the Jet Propulsion Laboratory, California Institute of Technology, under a contract with the National Aeronautics and Space Administration (NASA).

11. References

Altamimi, Z., P. Rebischung, L. Metivier, and C. Xavier (2016), ITRF2014: A new release of the International Terrestrial Reference Frame modeling nonlinear station motions, J. Geophys. Res. Solid Earth, 121, doi:10.1002/2016JB013098.

Beckley, B.D, P.S. Callahan, D. W. Hancock III, G. T. Mitchum and R. D. Ray (2017): On the "Cal-Mode" Correction to TOPEX Satellite Altimetry and Its Effect on the Global Mean Sea Level Time Series, J. Geophys. Res – Oceans, https://doi.org/10.1002/2017JC013090. See also the poster at https://mediatum.ub.tum.de/doc/1523987/file.pdf

Bretherton, F., R. Davis and C. Fandry (1976). A technique for objective analysis and design of oceanographic experiments, applied to MODE73. Deep Sea Research, v23, pp 559-582.

Cressie N. and C.K.Wikle (2011) Statistics for spatio-temporal data. J. Wiley. ISBN-13: 978- 0471692744

Chelton, D.B., Schlax, M.G. and Samelson, R.M., 2011a. Global observations of nonlinear mesoscale eddies. Progress in oceanography, 91(2), pp.167-216.

Chelton, D.B., Gaube, P., Schlax, M.G., Early, J.J. and Samelson, R.M., 2011. The influence of nonlinear mesoscale eddies on near-surface oceanic chlorophyll. Science, 334(6054), pp.328-332.

Desai, S., J. Wahr, B. Beckley, Revisiting the pole tide for and from satellite altimetry, Journal of Geodesy, 89(8), 747-842, 2015. DOI 10.1007/s00190-015-0848-7

Desai, S. D., W. Bertiger, B. Haines, and A. Sibois, Evaluation of the use of high-rate tracking data for Jason-3 GPS-based precise orbit determination, 2020 Ocean Surface Topography Science Team Meeting, October 19-23, 2020.

Ducet, N., P.-Y. Le Traon, and G. Reverdin, 2000: Global highresolution mapping of ocean circulation from TOPEX/Poseidon and ERS-1 and-2. J. Geophys. Res., 105, 19 477–19 498, doi:10.1029/2000JC900063.

Gaspar, P., F. Ogor, P. Y. Le Traon, and O. Z. Zanife (1994), Estimating the sea state of the TOPEX and Poseidon altimeters from crossover differences, J. Geophys. Res., 99, 24,981 – 24,994.

Hamlington, B.D., Cheon, S.H., Piecuch, C.G., Karnauskas, K.B., Thompson, P.R., Kim, K.Y., Reager, J.T., Landerer, F.W. and Frederikse, T., 2019a. The dominant global modes of recent internal sea level variability. *Journal of Geophysical Research: Oceans*, *124*(4), pp.2750-2768

Hamlington, B. D., Fasullo, J. T., Nerem, R. S., Kim, K. Y., & Landerer, F. W. (2019b). Uncovering the pattern of forced sea level rise in the satellite altimeter record. *Geophysical Research Letters*, *46*(9), 4844-4853.

Jacobs, G. and M. Wooten, 2013: A multiscale analysis from satellite altimeter observations, 2013 *Ocean Surface Topography Science Team Meeting, Boulder, CO.*

Le Traon, P-Y and G. Dibarboure, 2002 Velocity Mapping Capabilities of Present and Future Altimeter Missions: The Role of High-Frequency Signals JTECH vol 19, pp 2077-2087,

Le Traon, P-Y, F. Nadal, and N. Ducet, 1998 An Improved Mapping Method of Multisatellite Altimeter Data J. of Atmospheric and Oceanic Techn, Vol 15, p522-534,

Ray, R. D. and S.Y. Erofeeva (2014), Long-period tidal variations in the length of day, Journal of Geophysical Research: Solid Earth, 119, 1498-1509, doi:10.1002/2013JB010830.

Samelson, R.M., M. G. Schlax, And D. B. Chelton, 2014 Randomness, Symmetry, and Scaling of Mesoscale Eddy Life Cycles JPO vol 44, pp 1012-1029. DOI: 10.1175/JPO-D-13-0161.1

Scharroo, R., E. W. Leuliette, J. L. Lillibridge, D. Byrne, M. C. Naeije, and G. T. Mitchum, RADS: Consistent multi-mission products, in Proc. of the Symposium on 20 Years of Progress in Radar Altimetry, Venice, 20-28 September 2012, European Space Agency Special Publication, ESA SP-710, p. 4 pp., 2013.

Sokolov, S., and S. R. Rintoul, 2007 Multiple jets of the Antarctic Circumpolar Current south of Australia. J. Phys. Oceanogr., 37, 1394–1412.

Taburet, G., Sanchez-Roman, A., Ballarotta, M., Pujol, M.I., Legeais, J.F., Fournier, F., Faugere, Y. and Dibarboure, G., 2019. DUACS DT2018: 25 years of reprocessed sea level altimetry products. Ocean Science, 15(5), pp.1207-1224.

Tran, N., S. Philipps, J. C. Poisson, S. Urien, E. Bronner, and N. Picot (2012), Impact of GDR- D standards on SSB correction, Ocean Science Topography Science Team Meeting, Venice, Italy, 27-29 September 2012.

Tran, N., S. Labroue, S. Phillips, E. Bronner, and N. Picot (2019), Overview and Update of the Sea State Bias Corrections for the Jason-2, Jason-1, and TOPEX Missions. Mar. Geod. 33(S1): 348-362, 2010. DOI: 10.1080/01490419.2010.487788

Thompson, Andrew F.and Jean-Baptiste Sallee´ (2012) Jets and Topography: Jet Transitions and the Impact on Transport in the Antarctic Circumpolar Current JPO vol 42, p 956-972, DOI: 10.1175/JPO-D-11-0135.1

Willis, J.K., 2010. Can in situ floats and satellite altimeters detect long-term changes in Atlantic Ocean overturning? Geophysical research letters, 37(6).

Zaron E. D, 2019, Baroclinic tidal sea level from exact-repeat mission altimetry. *Journal of Physical Oceanography*, 49(1):193-210